

Search for Yukawa Production of a Light Neutral Higgs Boson at LEP

The OPAL Collaboration

Abstract

Within a Two-Higgs-Doublet Model (2HDM) a search for a light Higgs boson in the mass range of 4–12 GeV has been performed in the Yukawa process $e^+e^- \rightarrow b\bar{b}A/h \rightarrow b\bar{b}\tau^+\tau^-$, using the data collected by the OPAL detector at LEP between 1992 and 1995 in e^+e^- collisions at about 91 GeV centre-of-mass energy. A likelihood selection is applied to separate background and signal. The number of observed events is in good agreement with the expected background. Within a CP-conserving 2HDM type II model the cross-section for Yukawa production depends on $\xi_d^A = |\tan\beta|$ and $\xi_d^h = |\sin\alpha/\cos\beta|$ for the production of the CP-odd A and the CP-even h, respectively, where $\tan\beta$ is the ratio of the vacuum expectation values of the Higgs doublets and α is the mixing angle between the neutral CP-even Higgs bosons. From our data 95% C.L. upper limits are derived for ξ_d^A within the range of 8.5 to 13.6 and for ξ_d^h between 8.2 to 13.7, depending on the mass of the Higgs boson, assuming a branching fraction into $\tau^+\tau^-$ of 100%. An interpretation of the limits within a 2HDM type II model with Standard Model particle content is given. These results impose constraints on several models that have been proposed to explain the recent BNL measurement of the muon anomalous magnetic moment.

(To be submitted to Eur. Phys. J. C)

The OPAL Collaboration

G. Abbiendi², C. Ainsley⁵, P.F. Åkesson³, G. Alexander²², J. Allison¹⁶, G. Anagnostou¹, K.J. Anderson⁹, S. Arcelli¹⁷, S. Asai²³, D. Axen²⁷, G. Azuelos^{18,a}, I. Bailey²⁶, E. Barberio⁸, R.J. Barlow¹⁶, R.J. Batley⁵, P. Bechtel²⁵, T. Behnke²⁵, K.W. Bell²⁰, P.J. Bell¹, G. Bella²², A. Bellerive⁶, G. Benelli⁴, S. Bethke³², O. Biebel³², I.J. Bloodworth¹, O. Boeriu¹⁰, P. Bock¹¹, J. Böhme²⁵, D. Bonacorsi², M. Boutemour³¹, S. Braibant⁸, L. Brigliadori², R.M. Brown²⁰, H.J. Burckhart⁸, J. Cammin³, S. Campana⁴, R.K. Carnegie⁶, B. Caron²⁸, A.A. Carter¹³, J.R. Carter⁵, C.Y. Chang¹⁷, D.G. Charlton^{1,b}, P.E.L. Clarke¹⁵, E. Clay¹⁵, I. Cohen²², J. Couchman¹⁵, A. Csilling^{8,i}, M. Cuffiani², S. Dado²¹, G.M. Dallavalle², S. Dallison¹⁶, A. De Roeck⁸, E.A. De Wolf⁸, P. Dervan¹⁵, K. Desch²⁵, B. Dienes³⁰, M. Donkers⁶, J. Dubbert³¹, E. Duchovni²⁴, G. Duckeck³¹, I.P. Duerdoth¹⁶, E. Etzion²², F. Fabbri², L. Feld¹⁰, P. Ferrari¹², F. Fiedler⁸, I. Fleck¹⁰, M. Ford⁵, A. Frey⁸, A. Fürtjes⁸, D.I. Futyan¹⁶, P. Gagnon¹², J.W. Gary⁴, G. Gaycken²⁵, C. Geich-Gimbel³, G. Giacomelli², P. Giacomelli², M. Giunta⁴, J. Goldberg²¹, K. Graham²⁶, E. Gross²⁴, J. Grunhaus²², M. Gruwé⁸, P.O. Günther³, A. Gupta⁹, C. Hajdu²⁹, M. Hamann²⁵, G.G. Hanson¹², K. Harder²⁵, A. Harel²¹, M. Harin-Dirac⁴, M. Hauschild⁸, J. Hauschildt²⁵, C.M. Hawkes¹, R. Hawkings⁸, R.J. Hemingway⁶, C. Hensel²⁵, G. Herten¹⁰, R.D. Heuer²⁵, J.C. Hill⁵, K. Hoffman⁹, R.J. Homer¹, D. Horváth^{29,c}, K.R. Hossain²⁸, R. Howard²⁷, P. Hüntemeyer²⁵, P. Igo-Kemenes¹¹, K. Ishii²³, A. Jawahery¹⁷, H. Jeremie¹⁸, C.R. Jones⁵, P. Jovanovic¹, T.R. Junk⁶, N. Kanaya²⁶, J. Kanzaki²³, G. Karapetian¹⁸, D. Karlen⁶, V. Kartvelishvili¹⁶, K. Kawagoe²³, T. Kawamoto²³, R.K. Keeler²⁶, R.G. Kellogg¹⁷, B.W. Kennedy²⁰, D.H. Kim¹⁹, K. Klein¹¹, A. Klier²⁴, S. Kluth³², T. Kobayashi²³, M. Kobel³, T.P. Kokott³, S. Komamiya²³, R.V. Kowalewski²⁶, T. Krämer²⁵, T. Kress⁴, P. Krieger^{6,p}, J. von Krogh¹¹, D. Krop¹², T. Kuhl²⁵, M. Kupper²⁴, P. Kyberd¹³, G.D. Lafferty¹⁶, H. Landsman²¹, D. Lanske¹⁴, I. Lawson²⁶, J.G. Layter⁴, A. Leins³¹, D. Lellouch²⁴, J. Letts¹², L. Levinson²⁴, J. Lillich¹⁰, C. Littlewood⁵, S.L. Lloyd¹³, F.K. Loebinger¹⁶, J. Lu²⁷, J. Ludwig¹⁰, A. Macchiolo¹⁸, A. Macpherson^{28,l}, W. Mader³, S. Marcellini², T.E. Marchant¹⁶, A.J. Martin¹³, J.P. Martin¹⁸, G. Martinez¹⁷, G. Masetti², T. Mashimo²³, P. Mättig²⁴, W.J. McDonald²⁸, J. McKenna²⁷, T.J. McMahan¹, R.A. McPherson²⁶, F. Meijers⁸, P. Mendez-Lorenzo³¹, W. Menges²⁵, F.S. Merritt⁹, H. Mes^{6,a}, A. Michelini², S. Mihara²³, G. Mikenberg²⁴, D.J. Miller¹⁵, S. Moed²¹, W. Mohr¹⁰, T. Mori²³, A. Mutter¹⁰, K. Nagai¹³, I. Nakamura²³, H.A. Neal³³, R. Nisius⁸, S.W. O’Neale¹, A. Oh⁸, A. Okpara¹¹, M.J. Oreglia⁹, S. Orito²³, C. Pahl³², G. Pásztor^{8,i}, J.R. Pater¹⁶, G.N. Patrick²⁰, J.E. Pilcher⁹, J. Pinfold²⁸, D.E. Plane⁸, B. Poli², J. Polok⁸, O. Pooth⁸, A. Quadt³, K. Rabbertz⁸, C. Rembser⁸, P. Renkel²⁴, H. Rick⁴, N. Rodning²⁸, J.M. Roney²⁶, S. Rosati³, K. Roscoe¹⁶, Y. Rozen²¹, K. Runge¹⁰, D.R. Rust¹², K. Sachs⁶, T. Saeki²³, O. Sahr³¹, E.K.G. Sarkisyan^{8,m,n}, A.D. Schaile³¹, O. Schaile³¹, P. Scharff-Hansen⁸, M. Schröder⁸, M. Schumacher²⁵, C. Schwick⁸, W.G. Scott²⁰, R. Seuster^{14,g}, T.G. Shears^{8,j}, B.C. Shen⁴, C.H. Shepherd-Themistocleous⁵, P. Sherwood¹⁵, A. Skuja¹⁷, A.M. Smith⁸, G.A. Snow¹⁷, R. Sobie²⁶, S. Söldner-Rembold^{31,e}, S. Spagnolo²⁰, F. Spano⁹, M. Sproston²⁰, A. Stahl³, K. Stephens¹⁶, D. Strom¹⁹, R. Ströhmer³¹, L. Stumpf²⁶, B. Surrow²⁵, S. Tarem²¹, M. Tasevsky⁸, R.J. Taylor¹⁵, R. Teuscher⁹, J. Thomas¹⁵, M.A. Thomson⁵, E. Torrence¹⁹, D. Toya²³, T. Trefzger³¹, A. Tricoli², I. Trigger⁸, Z. Trócsányi^{30,f}, E. Tsur²², M.F. Turner-Watson¹, I. Ueda²³, B. Ujvári^{30,f}, B. Vachon²⁶, C.F. Vollmer³¹, P. Vannerem¹⁰,

M. Verzocchi¹⁷, H. Voss⁸, J. Vossebeld⁸, D. Waller⁶, C.P. Ward⁵, D.R. Ward⁵, P.M. Watkins¹,
A.T. Watson¹, N.K. Watson¹, P.S. Wells⁸, T. Wengler⁸, N. Wermes³, D. Wetterling¹¹
G.W. Wilson^{16,o}, J.A. Wilson¹, T.R. Wyatt¹⁶, S. Yamashita²³, V. Zacek¹⁸, D. Zer-Zion^{8,k}

¹School of Physics and Astronomy, University of Birmingham, Birmingham B15 2TT, UK

²Dipartimento di Fisica dell' Università di Bologna and INFN, I-40126 Bologna, Italy

³Physikalisches Institut, Universität Bonn, D-53115 Bonn, Germany

⁴Department of Physics, University of California, Riverside CA 92521, USA

⁵Cavendish Laboratory, Cambridge CB3 0HE, UK

⁶Ottawa-Carleton Institute for Physics, Department of Physics, Carleton University, Ottawa, Ontario K1S 5B6, Canada

⁸CERN, European Organisation for Nuclear Research, CH-1211 Geneva 23, Switzerland

⁹Enrico Fermi Institute and Department of Physics, University of Chicago, Chicago IL 60637, USA

¹⁰Fakultät für Physik, Albert Ludwigs Universität, D-79104 Freiburg, Germany

¹¹Physikalisches Institut, Universität Heidelberg, D-69120 Heidelberg, Germany

¹²Indiana University, Department of Physics, Swain Hall West 117, Bloomington IN 47405, USA

¹³Queen Mary and Westfield College, University of London, London E1 4NS, UK

¹⁴Technische Hochschule Aachen, III Physikalisches Institut, Sommerfeldstrasse 26-28, D-52056 Aachen, Germany

¹⁵University College London, London WC1E 6BT, UK

¹⁶Department of Physics, Schuster Laboratory, The University, Manchester M13 9PL, UK

¹⁷Department of Physics, University of Maryland, College Park, MD 20742, USA

¹⁸Laboratoire de Physique Nucléaire, Université de Montréal, Montréal, Quebec H3C 3J7, Canada

¹⁹University of Oregon, Department of Physics, Eugene OR 97403, USA

²⁰CLRC Rutherford Appleton Laboratory, Chilton, Didcot, Oxfordshire OX11 0QX, UK

²¹Department of Physics, Technion-Israel Institute of Technology, Haifa 32000, Israel

²²Department of Physics and Astronomy, Tel Aviv University, Tel Aviv 69978, Israel

²³International Centre for Elementary Particle Physics and Department of Physics, University of Tokyo, Tokyo 113-0033, and Kobe University, Kobe 657-8501, Japan

²⁴Particle Physics Department, Weizmann Institute of Science, Rehovot 76100, Israel

²⁵Universität Hamburg/DESY, II Institut für Experimental Physik, Notkestrasse 85, D-22607 Hamburg, Germany

²⁶University of Victoria, Department of Physics, P O Box 3055, Victoria BC V8W 3P6, Canada

²⁷University of British Columbia, Department of Physics, Vancouver BC V6T 1Z1, Canada

²⁸University of Alberta, Department of Physics, Edmonton AB T6G 2J1, Canada

²⁹Research Institute for Particle and Nuclear Physics, H-1525 Budapest, P O Box 49, Hungary

³⁰Institute of Nuclear Research, H-4001 Debrecen, P O Box 51, Hungary

³¹Ludwigs-Maximilians-Universität München, Sektion Physik, Am Coulombwall 1, D-85748 Garching, Germany

³²Max-Planck-Institute für Physik, Föhring Ring 6, 80805 München, Germany

³³Yale University, Department of Physics, New Haven, CT 06520, USA

^a and at TRIUMF, Vancouver, Canada V6T 2A3

^b and Royal Society University Research Fellow

^c and Institute of Nuclear Research, Debrecen, Hungary

^e and Heisenberg Fellow

^f and Department of Experimental Physics, Lajos Kossuth University, Debrecen, Hungary

^g and MPI München

ⁱ and Research Institute for Particle and Nuclear Physics, Budapest, Hungary

^j now at University of Liverpool, Dept of Physics, Liverpool L69 3BX, UK

^k and University of California, Riverside, High Energy Physics Group, CA 92521, USA

^l and CERN, EP Div, 1211 Geneva 23

^m and Universitaire Instelling Antwerpen, Physics Department, B-2610 Antwerpen, Belgium

ⁿ and Tel Aviv University, School of Physics and Astronomy, Tel Aviv 69978, Israel

^o now at University of Kansas, Dept of Physics and Astronomy, Lawrence, KS 66045, USA

^p now at University of Toronto, Dept of Physics, Toronto, Canada

1 Introduction

The search for the last missing particle predicted by the Standard Model, the Higgs boson, is one of the main topics in high energy physics at LEP. The Standard Model (SM) has been verified to a very high degree of precision but no Higgs boson has yet been discovered. Current searches at LEP in the Standard Model scenario [1] exclude Higgs bosons with masses m_{H^0} below 114.1 GeV at the 95% confidence level. Many proposed models extend the SM while preserving the good agreement with experimental data. A minimal extension of the SM, the Two-Higgs-Doublet Model (2HDM), has this property. In non-supersymmetric 2HDMs, Higgs bosons with small masses still cannot be excluded [2, 3]. The analysis presented here, a search for A and h in the mass range 4–12 GeV, provides new constraints on the parameter space of these models.

In the 2HDM, two complex Higgs doublets are introduced to generate the mass of the fermions:

$$\Phi_1 = \begin{pmatrix} \phi_1^+ \\ \phi_1^0 \end{pmatrix} \quad ; \quad \Phi_2 = \begin{pmatrix} \phi_2^+ \\ \phi_2^0 \end{pmatrix}. \quad (1)$$

One constraint for extended Higgs sectors is the experimental observation that the value of $\rho \equiv m_{W^\pm}^2 / (m_Z^2 \cos^2 \theta_W) \approx 1$. The condition of $\rho \approx 1$ is automatically met by models with only Higgs doublets.

There are several possible patterns for how the new fields may couple to fermions. Four types of 2HDMs are theoretically considered in order to avoid introducing flavour changing neutral currents (FCNC) [4]. The four types differ in the way the two Higgs fields Φ_1 and Φ_2 couple to fermions (see Table 1).

couples to	type I	type II	type III	type IV
down-type leptons	Φ_2	Φ_1	Φ_2	Φ_1
up-type quarks	Φ_2	Φ_2	Φ_2	Φ_2
down-type quarks	Φ_2	Φ_1	Φ_1	Φ_2

Table 1: *The couplings of the Higgs fields according to the four types of 2HDMs.*

In this analysis the CP-conserving 2HDM type II is considered where Φ_1 couples to the down-type and the Φ_2 couples to the up-type matter fields. This 2HDM predicts five physical Higgs bosons: two charged (H^\pm), two CP-even (H^0 , h) and one CP-odd (A) Higgs boson (the neutral Higgs bosons are often referred to as *scalar* and *pseudoscalar*, respectively). The Higgs sector of the general CP-conserving 2HDM has six free physical parameters [4] and can be parametrized by the masses m_{H^\pm} , m_{H^0} , m_h and m_A and two dimensionless parameters α and $\tan \beta$, with α being the mixing angle in the CP-even neutral Higgs sector, and $\tan \beta = v_2/v_1$ being the ratio of the two vacuum expectation values v_2 and v_1 .

The Higgs sector in the Minimal Supersymmetric Standard Model (MSSM) is a special case of a 2HDM type II model in which, due to relations imposed by supersymmetry, only two free

parameters remain (eg. $\tan\beta$ and α) at tree level in the Higgs sector. Direct searches at LEP in the MSSM scenario have set limits on the Higgs mass and its parameter space. For example in a parameter scan where the parameter combination was chosen to give a maximal predicted mass m_h , 95% C.L. limits have been set on the masses m_h and m_A larger than 88.4 GeV for $\tan\beta > 0.4$ [5].

2 Higgs Boson Production in e^+e^- Collisions

There are three main processes for Higgs production at Born level within the energy range covered by LEP, namely the Higgsstrahlung, associated production and Yukawa processes shown in Figure 1, of which only the first process is of importance in the Standard Model. In the Standard Model the Yukawa process is suppressed by the factor (m_f^2/m_h^2) , and the associated production of Higgs bosons is nonexistent. The cross-sections of the 2HDM are closely related

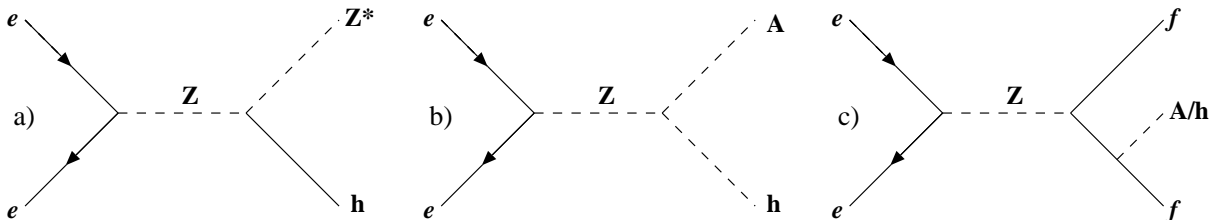


Figure 1: *The three Born level Higgs production processes in a 2HDM at LEP: The Higgsstrahlung process a), associated production b) and the Yukawa process c).*

to similar processes of the Standard Model:

$$\sigma(e^+e^- \rightarrow Z \rightarrow hZ^*) = \sigma_{\text{SM}}(e^+e^- \rightarrow Z \rightarrow H_{\text{SM}}Z^*) \sin^2(\beta - \alpha) \quad (2)$$

$$\sigma(e^+e^- \rightarrow Z \rightarrow hA) = \sigma_{\text{SM}}(e^+e^- \rightarrow Z \rightarrow \nu\bar{\nu}) \cos^2(\beta - \alpha) \lambda^{\frac{3}{2}} \quad (3)$$

where $\lambda = (1 - \kappa_h - \kappa_A)^2 - 4\kappa_h^2\kappa_A^2$ being a phase space factor, with $\kappa_i = m_i^2/m_Z^2$ [4].

In recent years there have been searches for the Standard Model Higgs boson as well as for MSSM Higgs bosons by all four LEP experiments [5]. The interpretation of the flavour independent Higgs search within the 2HDM in the mass range below approximately 40 GeV requires $\sin^2(\beta - \alpha)$ to be less than 0.2 [6]. For a sufficiently small $\sin^2(\beta - \alpha)$, the h produced through the Higgsstrahlung process can not be seen in the data collected at LEP due to the cross-section suppression factor (Eqn. 2). Associated production, if kinematically allowed, would be the dominant process for Higgs boson production. On the other hand a light Higgs boson which is produced only in the Yukawa process (A or h whichever is lighter) could have escaped discovery. Under the assumption that the Higgsstrahlung process is suppressed and associated production is kinematically forbidden, $m_A + m_h > \sqrt{s}$, the Yukawa process becomes the dominant process for Higgs production at LEP. This scenario can easily be realised in the general 2HDM since its parameters are not constrained theoretically [2, 3]. In this analysis we

concentrate on Higgs masses below the $2m_b$ threshold since previous analyses [7] are insensitive to such light Higgs bosons. We will also constrain ourselves to Higgs masses above the $2m_\tau$ threshold.

The cross-section of the Yukawa process [8]

$$\sigma_{\text{Yukawa}} \propto m_f^2 N_c \xi_f^2 \quad (4)$$

is proportional to the squared fermion mass, m_f^2 , the colour factor, N_c , of the emitting fermion, and an enhancement factor ξ_f^2 , which describes the coupling between the Higgs boson and the emitting fermion (see Table 2).

Higgs Type	Down Type Fermions	Up Type Fermions
A	$\xi_d^A = \tan \beta$	$\xi_u^A = 1/\tan \beta$
h	$\xi_d^h = -\sin \alpha / \cos \beta$	$\xi_u^h = \cos \alpha / \sin \beta$

Table 2: *The enhancement factor ξ_f depending on the type of the Higgs boson and the emitting fermion.*

The range of $\xi_d^{h/A}$ for which a detectable signal would be produced can be divided into two parts:

1. $\xi_d < 1$ (implies $\xi_u > 1$): An up-type quark pair $c\bar{c}$ radiates a Higgs boson decaying into $c\bar{c}$.
2. $\xi_d > 1$: A down-type quark pair $b\bar{b}$ radiates a Higgs boson decaying into $\tau^+\tau^-$.

In this analysis, only the $b\bar{b}\tau^+\tau^-$ final state is considered, since background suppression can be performed more efficiently using the clear signature of bottom decay, together with the missing energy and low-multiplicity signature of τ decays. In Figure 2 the respective numbers of expected events are shown as a function of ξ_d^h for the example of a CP-even Higgs with a mass of 4 GeV.

3 Search in the $b\bar{b}\tau^+\tau^-$ Channel

3.1 Data and Monte Carlo Samples

The present analysis is based on data collected with the OPAL detector [10] during the years 1992–1995, taken at centre-of-mass energies close to the Z peak. Although the integrated luminosity at LEP recorded at \sqrt{s} between 130 and 208 GeV is about a factor five higher than the luminosity around the Z peak, the number of produced b quarks is about a factor of 100 smaller in the higher-energy data. Therefore we only use data recorded at the Z peak at

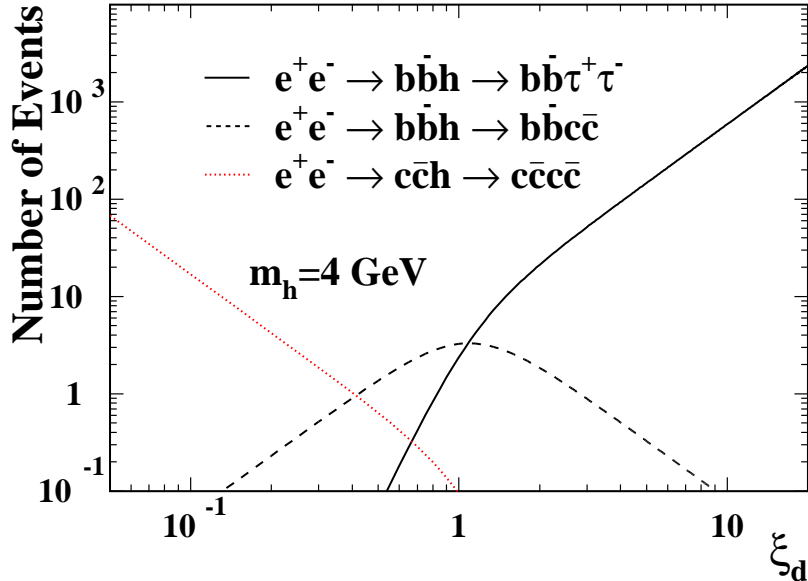


Figure 2: *The number of expected signal events for a scalar Higgs h with $m_h = 4 \text{ GeV}$ calculated for a luminosity of 113.1 pb^{-1} at $\sqrt{s} = m_Z$.*

centre-of-mass energies near 91 GeV to search for Yukawa production of Higgs bosons. The data collected at off-peak energies in the range between 89 GeV and 93 GeV are included to increase the available statistics. Since the characteristics of signal events do not depend on the precise center-of-mass energy, and since the background is completely dominated by SM hadronic Z decays, we can treat the data as if all were taken on-peak by rescaling the off-peak luminosity appropriately. For this we count the number of observed hadronic events [11] in the data. This number, efficiency corrected and divided by the peak cross-section for hadronic Z decays of 30.45 nb as measured by OPAL [12], then yields an effective on-peak luminosity of 113.1 pb^{-1} [13], from which about 12% is contributed by the data taken off-peak.

We consider three types of background classes, with the full detector response simulated as described in [14], using the following generators.

1. **Two-photon background**, generated with Vermaseren 1.01 [15] and PHOJET [16]

Two-photon production of hadronic final states is characterized by little visible energy in the detector. Usually, the e^+ and e^- escape undetected close to the beam axis, causing only a small amount of transverse momentum. The relatively large cross-section of this process nevertheless makes us consider it as a potential background. The Monte Carlo sample of about two million two-photon events corresponds to a luminosity of about four times the data luminosity.

2. **Four-fermion background**, generated with FERMISV [17] and grc4f [18]

The four-fermion background at LEP 1 mainly originates from Initial State Pair (ISP) and Final State Pair (FSP) radiation diagrams. This background class can be divided into two subclasses, the first containing four lepton final states and the second having $q\bar{q}f\bar{f}$ final states. The first subclass is eliminated by requiring the event to pass a general multihadronic selection [13]. The second class contains a small amount of irreducible $e^+e^- \rightarrow b\bar{b}\ell^+\ell^-$ background with a charged lepton pair, mainly from FSP radiation. The Monte Carlo sample of about 25000 four-fermion events corresponds to a luminosity of about eight times the data luminosity.

3. **$q\bar{q}$ background**, generated with Jetset 7.4 [19]

This class of background consists of events of the type $e^+e^- \rightarrow Z/\gamma \rightarrow q\bar{q}$. Events with gluons radiated off the quarks, especially $e^+e^- \rightarrow Z/\gamma \rightarrow b\bar{b}g(g)$, are very likely to have signal characteristics and represent the main background in this analysis. The Monte Carlo sample of about seven million processed $q\bar{q}$ events corresponds to a luminosity about two times the data luminosity. Generated Monte Carlo $q\bar{q}$ background samples for different detector setups are weighted according to the respective luminosity for the data.

Eighteen signal samples of 10000 events each with masses of $m_{h/A}=4-12$ GeV in one GeV steps were generated using a newly written Monte Carlo program based on [8]. The hadronisation is done with JETSET version 7.408 [19] together with OPAL specific modifications [20]. The decay of the tau leptons is simulated with the tau decay library TAUOLA [21]. These signal events are subjected to the same reconstruction and event selection as the real data.

3.2 Analysis Tools

In calculating the visible energies and momenta, E_{vis} and \vec{P}_{vis} , of individual jets and of the total event, “energy-flow objects” are formed from the charged tracks and calorimeter clusters [22]. To avoid double counting, the energies expected to be deposited in the calorimeters by the charged particles are subtracted from the energies of the associated calorimeter clusters.

In order to identify jets containing b hadron decays, three independent techniques using lifetime, high- p_t lepton characteristics and kinematic information are used. Artificial Neural Networks (ANN's) have been trained to combine several lifetime-sensitive tagging variables and kinematic variables. For each jet, the outputs of the lifetime ANN, the kinematic ANN, and the lepton tag are combined into a likelihood variable B which discriminates b-flavoured jets from c-flavoured jets and light quark jets [7].

3.3 Properties of Yukawa Production

One of the properties of Yukawa production is the hard energy spectrum of the emitted Higgs bosons. In Figure 3 the energy distributions of the A and h are shown. This leads to a high boost of the decay products of the Higgs particles and results in a small angle between the two τ 's in the detector. Consequently, the tracks of the decay products of the two τ 's can be reconstructed in one single low-multiplicity jet. In addition, two high-multiplicity jets are expected to be associated with the b quarks. Thus the expected topology of a signal event has a three jet signature. A simulated signal event is shown in Figure 4. In this analysis each event is forced into three jets using the Durham algorithm [9]. The jets are sorted according to their multiplicity, assuming that the jet with the lowest charged particle multiplicity (denoted 'Jet(3)') contains the two τ leptons from the Higgs decay.

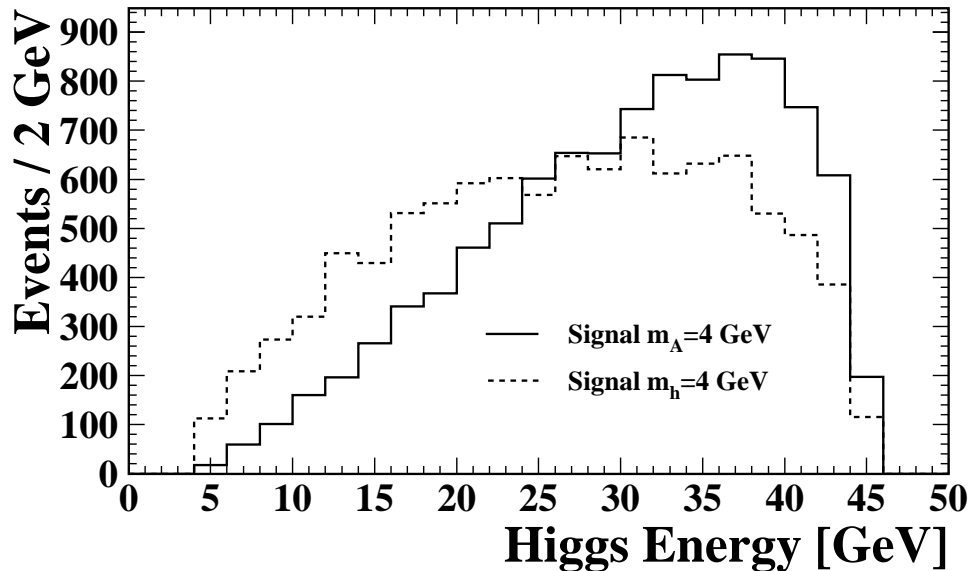


Figure 3: *The energy distribution of the Higgs boson with $m_{h/A} = 4$ GeV from 10000 Monte Carlo signal events at generator level.*

3.4 Event Selection

The event selection consists of two parts, a preselection and a subsequent likelihood selection. Since the unknown Higgs mass enters in the properties of the likelihood variables, the selection was performed and optimized separately for each of the nine simulated signal mass hypotheses.

The preselection consists of the eight cuts described below (see Figure 5).

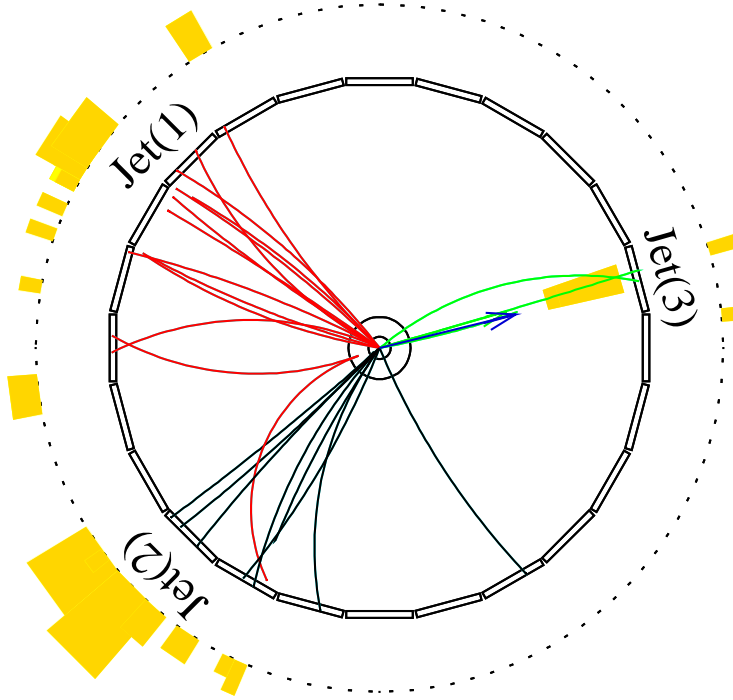


Figure 4: A characteristic simulated signal event $e^+e^- \rightarrow b\bar{b}A/h \rightarrow b\bar{b}\tau^+\tau^-$ reconstructed in the OPAL detector. Jet(1) and Jet(2) contain the tracks of the hadronized b quarks and Jet(3) contains the decay products of the Higgs boson. The missing momentum vector (dark grey arrow) points along the Jet(3) axis due to the undetected neutrinos in the decay of the τ 's.

0. General hadronic event selection as described in [13].
1. $E_{vis} < 90$ GeV. Due to the neutrinos from τ decays the signal events have missing energy in the detector. This cut on the visible energy primarily suppresses $q\bar{q}$ background.
2. $P_t(miss) > 3$ GeV. The cut on the transverse missing momentum in the event is additionally introduced to reduce two-photon background.
3. To suppress two-photon events further, we require the missing momentum vector to have $|\cos(\text{beam axis}, \vec{P}_{miss})| < 0.95$.
4. A two dimensional cut $3 \cdot C + \log(y_{32}) \geq -4.5$ on the event shape variables, C -value [23] and y_{32} [24], is introduced to suppress two-jet like events.
5. A large fraction of the missing momentum in the event is due to the undetectable neutrinos of the decaying τ 's in Jet(3). Therefore a cut on the angle between Jet(3) and \vec{P}_{miss} is introduced: $\cos(\text{Jet}(3), \vec{P}_{miss}) > -0.6$.
6. We require at least one identified electron or muon in Jet(3). Electrons are identified according to [25] and muons according to [26]. This cut is made to reduce $q\bar{q}$ background and to define efficient likelihood variables. The probability of two τ decays containing at

Cuts	Data	q \bar{q}	four-fermion	two-photon
(0)	338×10^4	338×10^4	887	346
(1)	196×10^4	198×10^4	545	236
(2)	131×10^4	128×10^4	357	123
(3)	125×10^4	123×10^4	330	54
(4)	622×10^3	599×10^3	198	43
(5)	400×10^3	383×10^3	125	32
(6)	292×10^2	307×10^2	39	5
(7)	142×10^2	141×10^2	22	1

Table 3: *The number of events selected and expected in the preselection. The three categories of background have been normalised to the data luminosity.*

least one charged lepton is approximately 60%. To ensure the correct efficiency modelling in the Monte Carlo a further cut on the lepton momentum, $P_l > 2$ GeV, is added.

7. $2 \leq N_{track} \leq 4$ in Jet(3). This cut on the charged multiplicity of Jet(3) is introduced in order to optimize the ratio of signal over square root of background after the likelihood selection.

As shown in Table 3, the observed number of data events and the expected background agree well at each step of the preselection. Of the background passing the general multihadronic selection (cut 0) about 2% of the four-fermion events, 0.4% of the q \bar{q} events and 0.3% of the two-photon events remain after the complete preselection, with the q \bar{q} background clearly being the dominant contribution. The signal selection efficiency, only weakly dependent of the Higgs boson mass, ranges from 11% to 17%, depending on the signal sample, as detailed for some typical masses in Table 4.

Cuts	Efficiency (%)	Efficiency (%)	Efficiency (%)	Efficiency (%)
	$m_A=4$ GeV	$m_A=10$ GeV	$m_h=4$ GeV	$m_h=10$ GeV
(1)	92.0	92.7	90.2	91.6
(2)	80.6	83.0	76.7	81.4
(3)	78.7	80.8	74.9	79.4
(4)	64.5	73.9	54.9	71.2
(5)	54.8	65.4	43.8	60.7
(6)	19.2	22.2	14.2	19.3
(7)	16.2	17.4	11.2	14.7

Table 4: *The efficiency of the preselection for selected Higgs masses.*

From reference histograms of eight variables, listed below, we define signal likelihood selections for each mass hypothesis, both for the h and the A Higgs boson. Due to the overwhelming dominance of the q \bar{q} background, we use a single inclusive background class. The eight reference histograms are (see Figure 6):

1. B_1 . The ‘b-ness’ of the jet with the highest multiplicity. This value is defined as

$$B_1 = \frac{L_b}{L_b + L_c + L_{uds}}. \quad (5)$$

Here L_b , L_c and L_{uds} are likelihood values for bottom, charm and light flavour jets respectively [7].

2. B_2 . The ‘b-ness’ value of the jet with the second highest multiplicity.

3. M_{vis} . The measured invariant mass of the event.

4. The C -value of the event [23].

5. $(P_1 + P_2)/E_{jet}$ in Jet(3). The sum of the momenta of the two tracks in Jet(3) with the highest momentum divided by the measured energy in Jet(3).

6. P_t . The transverse momentum of the event, with respect to the beam axis.

7. $\log(y_{32})$. The logarithm of the y_{32} value of the event [24].

8. $\cos(\text{Jet}(1), \text{Jet}(2))$. Cosine of the angle between the jet with the highest multiplicity (Jet(1)) and the one with the second highest multiplicity (Jet(2)).

The likelihood distributions are shown in Figure 7. The likelihood cuts are determined separately for each Higgs type and mass hypothesis in a compromise to achieve a good expected limit, calculated with Monte Carlo experiments, and a smooth behavior of efficiency and expected number of backgrounds as a function of the Higgs mass. After the likelihood cut the data are in good agreement with background Monte Carlo simulation (see Table 5 and Table 6).

Mass(A) (GeV)	LH cut	Data Events	Total background Events	Efficiency %
4	0.985	12	14.9±2.9±1.6	3.4±0.2±0.1
5	0.985	17	16.0±3.1±1.7	3.5±0.2±0.1
6	0.985	13	16.6±3.1±1.7	3.7±0.2±0.1
7	0.987	14	13.8±2.8±1.4	3.8±0.2±0.2
8	0.990	13	17.8±3.3±1.9	3.7±0.2±0.1
9	0.990	11	15.1±3.0±1.6	3.9±0.2±0.2
10	0.990	11	17.6±3.2±1.8	3.8±0.2±0.2
11	0.990	13	19.1±3.3±2.0	4.0±0.2±0.2
12	0.992	13	18.3±3.3±1.9	3.9±0.2±0.2

Table 5: *The number of selected A candidate events after the likelihood cut.*

Mass(h) (GeV)	LH cut	Data Events	Total background Events	Efficiency %
4	0.965	38	46.9±5.1±4.8	2.8±0.2±0.1
5	0.970	41	36.9±4.6±3.8	3.1±0.2±0.1
6	0.975	26	29.0±4.1±3.0	2.8±0.2±0.1
7	0.980	22	20.5±3.4±2.1	3.2±0.2±0.1
8	0.985	18	12.7±2.7±1.3	3.1±0.2±0.1
9	0.987	16	15.3±3.0±1.6	3.2±0.2±0.1
10	0.985	15	17.9±3.2±1.8	3.0±0.2±0.1
11	0.990	11	10.1±2.4±1.0	3.3±0.2±0.1
12	0.993	9	9.9±2.4±1.0	3.3±0.2±0.1

Table 6: *The number of selected h candidate events after the likelihood cut.*

4 Systematic Studies

In order to estimate systematic uncertainties, the following sources of uncertainty are varied in the Monte Carlo, one at a time, and the analysis is redone with the adjusted samples to calculate the difference in the background expectation and the efficiency with respect to the standard analysis. For variations done in two directions, with respect to the central value, the largest deviation in expected background and efficiency after re-analysis is taken as the systematic uncertainty. The following sources of uncertainty were studied:

- The systematic error contributed by the b-tagging due to track resolution modelling. This was estimated with a variation of the track parameters $\phi_0 \pm 5\%$, $d_0 \pm 5\%$, $z_0 \pm 10\%$ as described in [27]. This variation particularly influences the values of track- and secondary vertex significances (d/σ_d and l/σ_l) which are important variables for the b-tagging procedure.
- The uncertainty in the b-quark fragmentation function [28] is estimated by varying ϵ_b by $\pm 25\%$ around a central value of $\epsilon_b = 0.0038$ [29]. A smaller (higher) value of ϵ_b corresponds to a harder (softer) B-hadron spectrum.
- Description of the kinematic variables used in the likelihood selection. The kinematic likelihood variables in the Monte Carlo were shifted to match the mean of the data. After the shift on the variable the selection is reapplied and the deviations in the expected background and efficiency are taken as systematic errors.
- The B-hadron charged decay multiplicity uncertainty [30].

The systematic deviations are calculated separately for the two different hypotheses on Higgs type (A and h) after a likelihood cut at 0.8 to ensure that statistical contributions to the estimated systematic errors are minimal.

Variation of	A Selection		h Selection	
	Signal eff. %	q \bar{q} background Events	Signal eff. %	q \bar{q} background Events
Track parameters	0.2	4.1	2.4	1.7
ϵ_b	2.7	8.3	1.7	9.2
B multiplicity	1.8	1.8	1.8	1.8
M_{vis}	0.3	2.6	0.9	1.8
$(P_1 + P_2)/E$	0.3	0.3	0.1	0.2
C -value	0.6	3.4	0.8	2.7
P_t	0.1	0.6	0.1	0.5
$\log(y_{32})$	0.5	0.8	0.2	0.2
$\cos(\text{Jet}(1), \text{Jet}(2))$	1.7	1.1	0.3	1.1
τ correlations	1.3	1.5	1.3	1.5
Total	4.0	10.5	3.9	10.3

Table 7: *Relative change of the signal efficiency and number of expected background events for the selection of A and h at a likelihood cut, $L > 0.8$. The total value expresses the quadratically added contributions.*

Furthermore the analysis for one typical Higgs hypothesis ($m_h=5$ GeV) was redone under the assumption of 100% correlated helicity states of the τ 's. The deviation of 1.3% for signal and 1.5% for background expectation were included as a source of systematic uncertainty. The contributions to the systematic uncertainty are broken down for the analyses in Table 7.

Adding in quadrature the statistical uncertainties and the uncertainties from the above sources yields the total errors, listed in Table 5 and Table 6, on the selection efficiency and background rates for all nine masses of A and h. The uncertainty due to the b-fragmentation function is the highest contribution.

5 Limits on $\xi^{h/A}$ in the 2HDM Type II

The results of the selection with systematic and statistical errors are listed in Table 5 for the A and in Table 6 for the h.

2HDM Type II limits are determined for the cross-section of the process $e^+e^- \rightarrow Z \rightarrow b\bar{b}\tau^+\tau^-$. Due to the dependence of the cross-section (Eqn. 4) on the enhancement factor $\xi_d^{h/A}$, a limit on ξ is obtained by calculating N_{95} , the 95% C.L. upper limit on the rate of accepted signal events in the data, according to [31], and adjusting for the efficiency, cross section, and luminosity.

The total error on the efficiency and on the background estimation are convoluted into the limit according to [32]. For the mass points between the measured ones, in one GeV steps from 4 to 12 GeV, the limit is linearly interpolated from the two neighbouring measurements. Com-

paring limits obtained with analyses optimized to neighbouring mass points, the uncertainty of the interpolation was estimated to be less than 0.5 units in ξ .

Type	$m_{h/A}$ GeV	4	5	6	7	8	9	10	11	12
A	expected ξ_d^{95}	9.5	10.3	11.0	11.1	12.9	13.4	14.4	15.5	16.6
A	observed ξ_d^{95}	8.5	11.0	9.6	11.5	10.7	11.0	11.3	12.3	13.6
h	expected ξ_d^{95}	10.2	10.3	11.3	10.8	10.5	12.1	13.7	11.9	12.9
h	observed ξ_d^{95}	8.2	11.8	10.4	11.8	13.7	12.6	12.6	12.7	12.9

Table 8: *The upper limit on ξ in a 2HDM Type II model for masses $m_{Higgs} = 4$ GeV to $m_{Higgs} = 12$ GeV at 95% C.L. calculated assuming 100% branching ratio of the A (upper part) and h (lower part) into $\tau^+\tau^-$.*

Assuming a branching ratio of 100% for Higgs boson decays into $\tau^+\tau^-$ the limits on $\xi_d^{h/A}$ are shown in Figure 8(a) for A production and in Figure 8(b) for h production, and are summarised in Table 8.

In a 2HDM model with Standard Model particle content, the Higgs branching ratio into $\tau^+\tau^-$ for $\xi_d \approx 10$ is about 85% for Higgs masses between 4 and 9.4 GeV. In the mass range from 9.4 GeV to 11.0 GeV the branching ratios are very much influenced by mixing of the Higgs bosons h and A with $b\bar{b}$ bound states with the same quantum numbers (see Table 9). We have therefore calculated the branching ratios of the Higgs into $\tau^+\tau^-$ according to reference [33]. The limits derived within this model are shown in Figure 9(a) and (b) for CP-odd and CP-even Higgs production, respectively. The observed structure, in particular at higher Higgs boson masses, is a consequence of the behaviour of the branching ratio in this particular model.

state n	η Mass GeV	χ_0 Mass GeV
1	9.412	9.860
2	9.992	10.235
3	10.340	
4	10.570	
5	10.846	
6	11.014	

Table 9: *The mass of the η states assumed to mix with the pseudoscalar A and of the χ_0 states assumed to mix with the scalar h, taken from [33].*

6 Implications for the Muon Anomalous Magnetic Moment

Recent measurements of the anomalous magnetic moment, $a_\mu = \frac{1}{2}(g - 2)_\mu$, of the muon have given a result which deviates from the Standard Model expectation by $\approx 400 \times 10^{-11}$, corresponding to about 2.6 standard deviations [34]. Depending on the estimation of the hadronic contribution to the muon anomalous magnetic moment, the 90% C.L. ranges for the contribution of New Physics $\delta a_\mu(\text{NP})$ are:

$$215 \times 10^{-11} \leq \delta a_\mu(\text{NP}) \leq 637 \times 10^{-11} \quad [35] \quad (6)$$

$$170 \times 10^{-11} \leq \delta a_\mu(\text{NP}) \leq 690 \times 10^{-11} \quad [36] \quad (7)$$

$$112 \times 10^{-11} \leq \delta a_\mu(\text{NP}) \leq 573 \times 10^{-11} \quad [37] \quad (8)$$

Light Higgs bosons A and h could form a part of a_μ via loop diagrams. A one-loop calculation [38] predicts positive contributions $\delta a_\mu^I(\text{h}) > 0$ for the h, and negative contributions $\delta a_\mu^I(\text{A}) < 0$ for the A. The two-loop terms, due to the stronger coupling of the Higgs fields to loops with heavy quarks, turn out to be larger in magnitude than the one-loop terms, and of opposite sign [39], giving a total positive contribution $\delta a_\mu^{II}(\text{A}) > 0$ for the A, as shown with indicated isolines in Figure 9 (a) [40]. However, the two-loop terms gives a total negative contribution $\delta a_\mu^{II}(\text{h}) < 0$ for the h, thus suggesting that the h can not account for the BNL observation. We show in Figure 9 (b) only the isolines of the contribution from the earlier one-loop calculation [41] which resulted in a positive value of $\delta a_\mu^I(\text{h})$. Our data exclude positive contributions $\delta a_\mu^I(\text{h}) > 100 \times 10^{-11}$ for h masses between 4.0 and 10.7 GeV at the one-loop level, and $\delta a_\mu^{II}(\text{A}) > 100 \times 10^{-11}$ for A masses between 4.0 and 9.9 GeV at the two-loop level. Similar limits have been derived from radiative Υ decays [40, 42] for h/A masses lighter than about 8 GeV, with, however, large QCD uncertainties.

In reference [41] and [40] the authors have suggested that a light Higgs boson could fully account for the observed deviation of the measured $(g - 2)_\mu$ from the Standard Model expectation. In a scenario without contributions of other new particles, eg. gauginos, and assuming that either h or A is heavy enough to render associated Ah production inaccessible at LEP, only the lighter of the two Higgs bosons would sizeably contribute. For a light h, one has to assume in addition $\sin(\beta - \alpha) \approx 0$ to explain its non-observation in the Standard Model search for the Higgsstrahlung process. The experimental results of this analysis can be interpreted in such a scenario and would rule out (using the one-loop calculation [41]) a light h in the mass range of 4–10.7 GeV, and (using the two-loop calculation [39]) a light A in the mass range from 4–9.9 GeV as the only source of the discrepancy in the $(g - 2)_\mu$ measurement for all three 90% C.L. ranges listed above.

7 Conclusion

The Yukawa production of light neutral Higgs bosons in the channel $e^+e^- \rightarrow b\bar{b}A/h \rightarrow b\bar{b}\tau^+\tau^-$ is studied. The search presented here, based on data collected by OPAL at $\sqrt{s} \approx m_Z$ in the years 1992 to 1995, has not revealed any significant excess over the expected background. Limits on the Yukawa production of a light Higgs with masses in the range of 4 GeV to 12 GeV have been set at 95% C.L. New limits on the parameters $\xi_d^A = |\tan\beta|$ and $\xi_d^h = |\sin\alpha/\cos\beta|$ are presented for A and h production, respectively. Assuming a branching ratio to $\tau^+\tau^-$ of 100% , upper limits for ξ_d^A can be set within the range of 8.5 to 13.6 and for ξ_d^h between 8.2 to 13.7, depending on the mass of the Higgs boson. In a 2HDM type II model with Standard Model particle content similar limits are obtained up to masses of 9.4 GeV. Above 9.4 GeV the mixing of the Higgs bosons h and A with $b\bar{b}$ bound states with the same quantum numbers, especially for the CP-odd A, results in weaker limits in certain mass ranges. The experimental result of this analysis restricts the contribution to the anomalous magnetic moment of the muon for a light h in the mass range of 4–10.7 GeV (using one-loop calculation [38]) and for a light A in the mass range from 4–9.9 GeV (using the two-loop calculation of [39]) to $\delta a_\mu(\text{Higgs}) < 100 \times 10^{-11}$ at the 95% C.L.

8 Acknowledgements

We particularly wish to thank the SL Division for the efficient operation of the LEP accelerator at all energies and for their close cooperation with our experimental group. We thank our colleagues from CEA, DAPNIA/SPP, CE-Saclay for their efforts over the years on the time-of-flight and trigger systems which we continue to use. We also gratefully thank A. Dedes and M. Krawczyk for valuable support on theoretical issues. In addition to the support staff at our own institutions we are pleased to acknowledge the
Department of Energy, USA,
National Science Foundation, USA,
Particle Physics and Astronomy Research Council, UK,
Natural Sciences and Engineering Research Council, Canada,
Israel Science Foundation, administered by the Israel Academy of Science and Humanities,
Minerva Gesellschaft,
Benozio Center for High Energy Physics,
Japanese Ministry of Education, Science and Culture (the Monbusho) and a grant under the Monbusho International Science Research Program,
Japanese Society for the Promotion of Science (JSPS),
German Israeli Bi-national Science Foundation (GIF),
Bundesministerium für Bildung und Forschung, Germany,
National Research Council of Canada,
Research Corporation, USA,
Hungarian Foundation for Scientific Research, OTKA T-029328, T023793 and OTKA F-023259.

References

- [1] ALEPH, DELPHI, L3, OPAL Collaborations and the LEP working group for Higgs boson searches, *Search for the Standard Model Higgs Boson at LEP*, CERN-EP/2001-055 (2001).
- [2] M. Krawczyk, *Acta Phys. Polon.* **B29** (1998) 3543.
- [3] P.H. Chankowski, M. Krawczyk *et al.*, *Eur. Phys. J* **C11** (1999) 661.
- [4] J. Gunion *et al.*, *The Higgs Hunter's Guide*, Addison-Wesley (1990).
- [5] ALEPH, DELPHI, L3, OPAL Collaborations and the LEP working group for Higgs boson searches, *Searches for Higgs Bosons: Preliminary Combined Results Using LEP Data Collected at Energies Up To 202 GeV*, CERN-EP/2000-055 (2000) 28.
- [6] The OPAL Collaboration, G. Abbiendi *et al.*, *Eur. Phys. J.* **C18** (2001) 425.
- [7] The OPAL Collaboration, G. Abbiendi *et al.*, *Eur. Phys. J.* **C12** (2000) 567.
- [8] J. Kalinowski and M. Krawczyk, *Acta Phys. Polon.* **B27** (1996) 961.
- [9] Y. Dokshitzer, *J. Phys.* **G17** (1991) 1537.
- [10] The OPAL Collaboration, K. Ahmet *et al.*, *Nucl. Instrum. Meth.* **A305** (1991) 275.
- [11] The OPAL Collaboration, G. Alexander *et al.*, *Z. Phys.* **C52** (1991) 175.
- [12] The OPAL Collaboration, G. Abbiendi *et al.*, *Eur. Phys. J.* **C19** (2001) 587.
- [13] The OPAL Collaboration, R. Akers *et al.*, *Z. Phys.* **C65** (1995) 17.
- [14] The OPAL Collaboration, J. Allison *et al.*, *Nucl. Instrum. Meth.* **A317** (1992) 47.
- [15] J.A.M. Vermaseren, *Nucl. Phys.* **B229** (1983) 347.
- [16] R. Engel, *Z. Phys.* **C66** (1995) 203;
R. Engel and J. Ranft, *Phys. Rev.* **D54** (1996) 4244.
- [17] J. Hilgart, R. Kleiss and F. Le Diberder, *Comp. Phys. Comm.* **75** (1993) 191.
- [18] J. Fujimoto *et al.*, *Comp. Phys. Comm.* **100** (1997) 128.
- [19] T. Sjöstrand, *High-energy-physics event generation with PYTHIA 5.7 and JETSET 7.4*, *Comp. Phys. Comm.* **82** (1994) 74.
- [20] The OPAL Collaboration, G. Alexander *et al.*, *Z. Phys.* **C69** (1996) 543;
The OPAL Collaboration, J. Allison *et al.*, *Nucl. Instrum. Meth.* **A317** (1992) 47.
- [21] S. Jadach, Z. Was *et al.*, *Comp. Phys. Comm.* **76** (1993) 361.
- [22] The OPAL Collaboration, K. Ackerstaff *et al.*, *Eur. Phys. J.* **C2** (1998) 213.

- [23] G. Paris, Phys. Lett. **B74** (1978) 65.
- [24] S. Catani *et al.*, Phys. Lett. **B269** (1991) 432.
- [25] The OPAL collaboration, G. Alexander *et al.*, Z. Phys. **C70** (1996) 357.
- [26] The OPAL Collaboration, M.Z. Akrawy *et al.*, Phys. Lett. **B263** (1991) 311.
- [27] The OPAL Collaboration, G. Abbiendi *et al.*, Eur. Phys. J. **C12** (2000) 567.
- [28] C. Peterson *et al.*, Phys. Rev. **D27** (1983) 105.
- [29] ALEPH, DELPHI, L3, OPAL, CDF and SLD Collaborations, *Combined results on b -hadron production rates, lifetimes, oscillations and semileptonic decays*, CERN-EP/2000-096 (2000).
- [30] The OPAL Collaboration, R. Akers *et al.*, Z. Phys. **C61** (1994) 209.
- [31] Particle Data Group, Phys. Rev. **D54** (1996) 1.
- [32] R. Cousins and V. Highland, Nucl. Instrum. Meth. **A320** (1992) 331.
- [33] M. Drees and K.-I. Hikasa, Phys. Rev. **D41** (1990) 1547.
- [34] Muon ($g-2$) Collaboration, H.N. Brown *et al.*, Phys. Rev. Lett. **86** (2001) 2227.
- [35] A. Czarnecki and W.J. Marciano, Phys. Rev. **D64** (2001) 013014.
- [36] M. Davier and A. Höcker, Phys. Lett. **B435** (1998) 427.
- [37] S. Narison, *Muon and tau anomalies updated*, hep-ph/0103199v3 (2001).
- [38] J.P. Leveille, Nucl. Phys. **B137** (1978) 63.
- [39] D. Chang, W.-F. Chang *et al.*, Phys. Rev. **D63** (2001) 091301; K. Cheung, C.-H. Chou *et al.*, *Muon Anomalous Magnetic Moment, Two-Higgs-Doublet Model, and Supersymmetry*, hep-ph/0103183.
- [40] M. Krawczyk, *The new $(g-2)_\mu$ measurement and limit on the light Higgs bosons in 2HDM (II)*, hep-ph/0103223v3 (Submitted to Phys. Rev. **D**).
- [41] A. Dedes and H.E. Haber, JHEP **0105** (2001) 6.
- [42] CUSB Collaboration, P. Franzini *et al.*, Phys. Rev. **D35** (1987) 2883.

OPAL

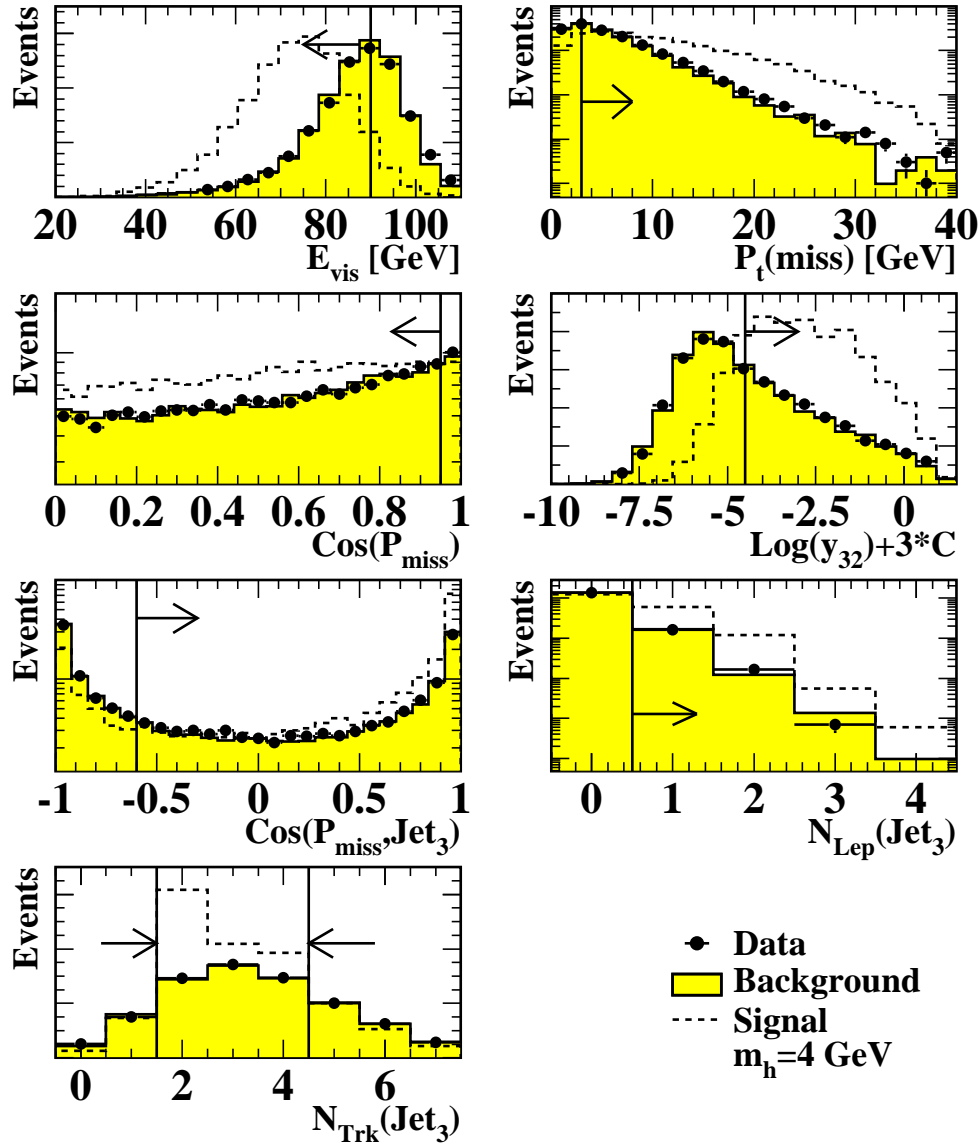


Figure 5: The preselection variables and their impact on processed data. The points with error bars are data, while the solid histogram is the simulation of the $q\bar{q}$ background normalised to the recorded luminosity. The dashed line represents a simulated signal of a scalar Higgs with $m_h = 4$ GeV scaled arbitrarily for better visibility. The arrows indicate the cuts made on the variables.

OPAL

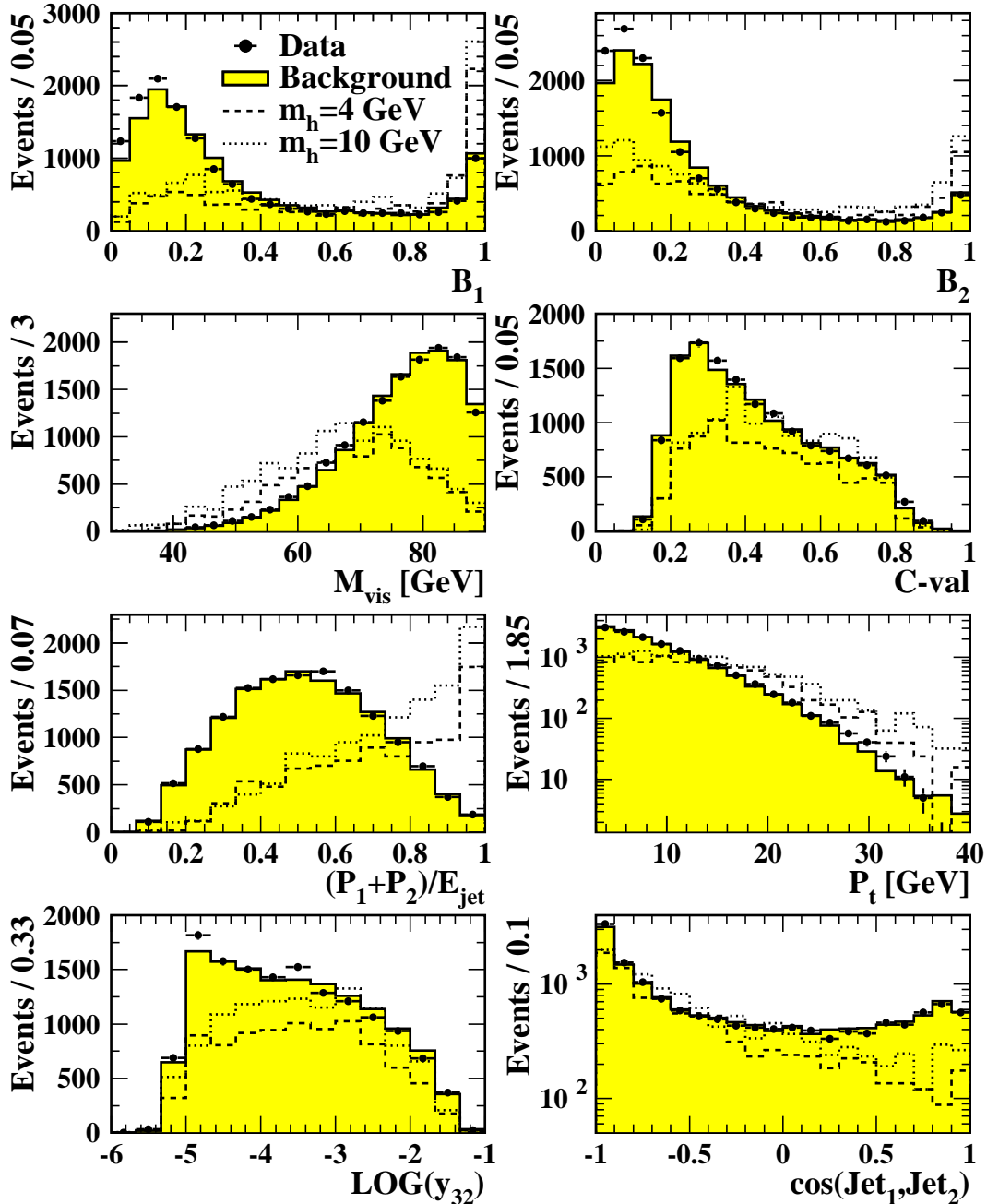


Figure 6: *Distributions used in the likelihood selection for preselected events and two hypothetical h Higgs masses. The points with error bars are data. The solid line is simulated background normalised to the recorded data. The dashed (dotted) line is a simulated Higgs boson h at a mass $m_{\text{Higgs}} = 4$ GeV ($m_{\text{Higgs}} = 10$ GeV) scaled arbitrarily for better visibility.*

OPAL

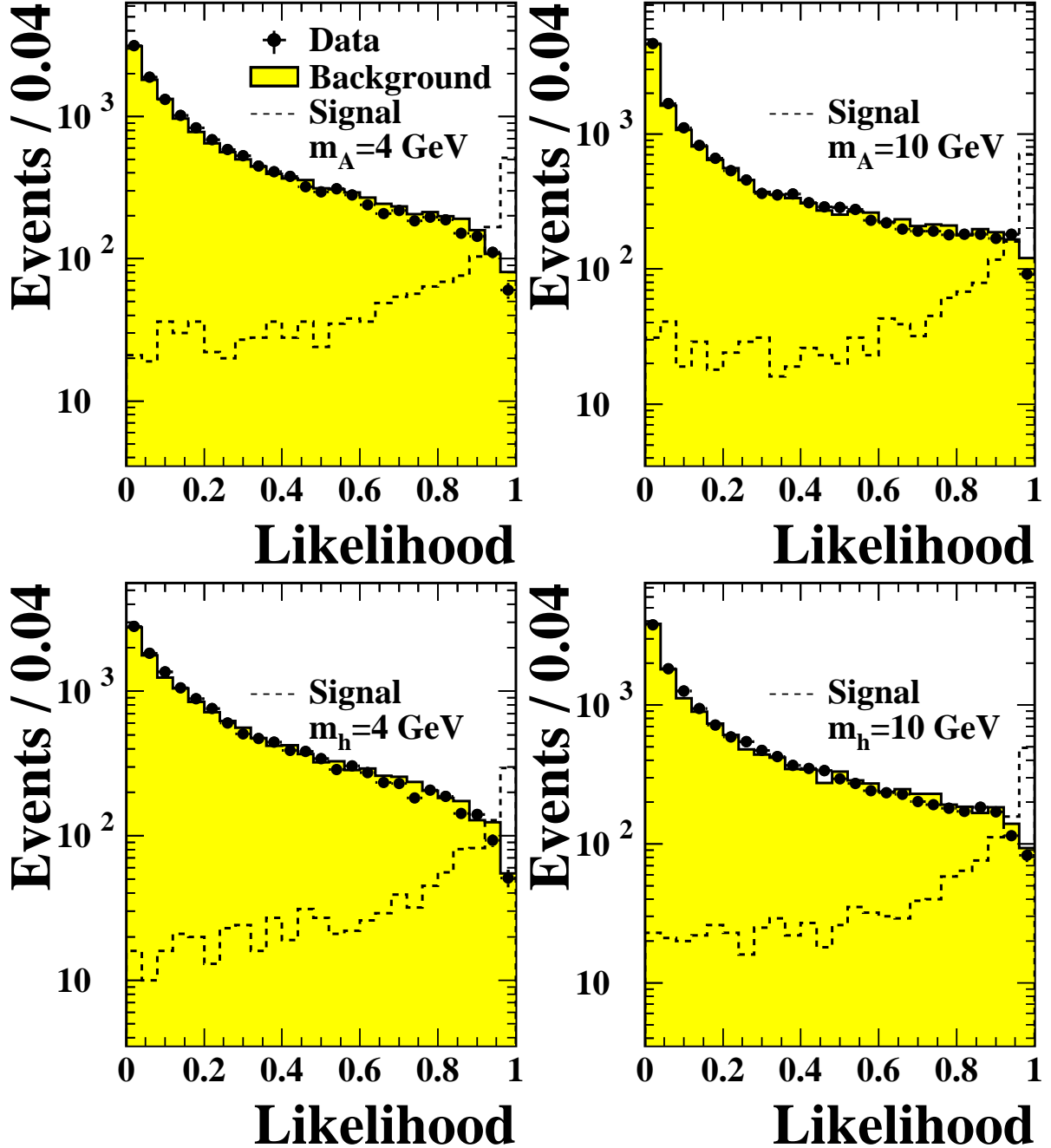


Figure 7: Likelihood distributions for the selection of a CP-odd Higgs A with masses of 4 and 10 GeV and for a CP-even Higgs h with masses of 4 and 10 GeV. The points with error bars are data. The solid line is simulated background normalised to the recorded luminosity. The dashed line is a simulated Higgs boson scaled arbitrarily for better visibility.

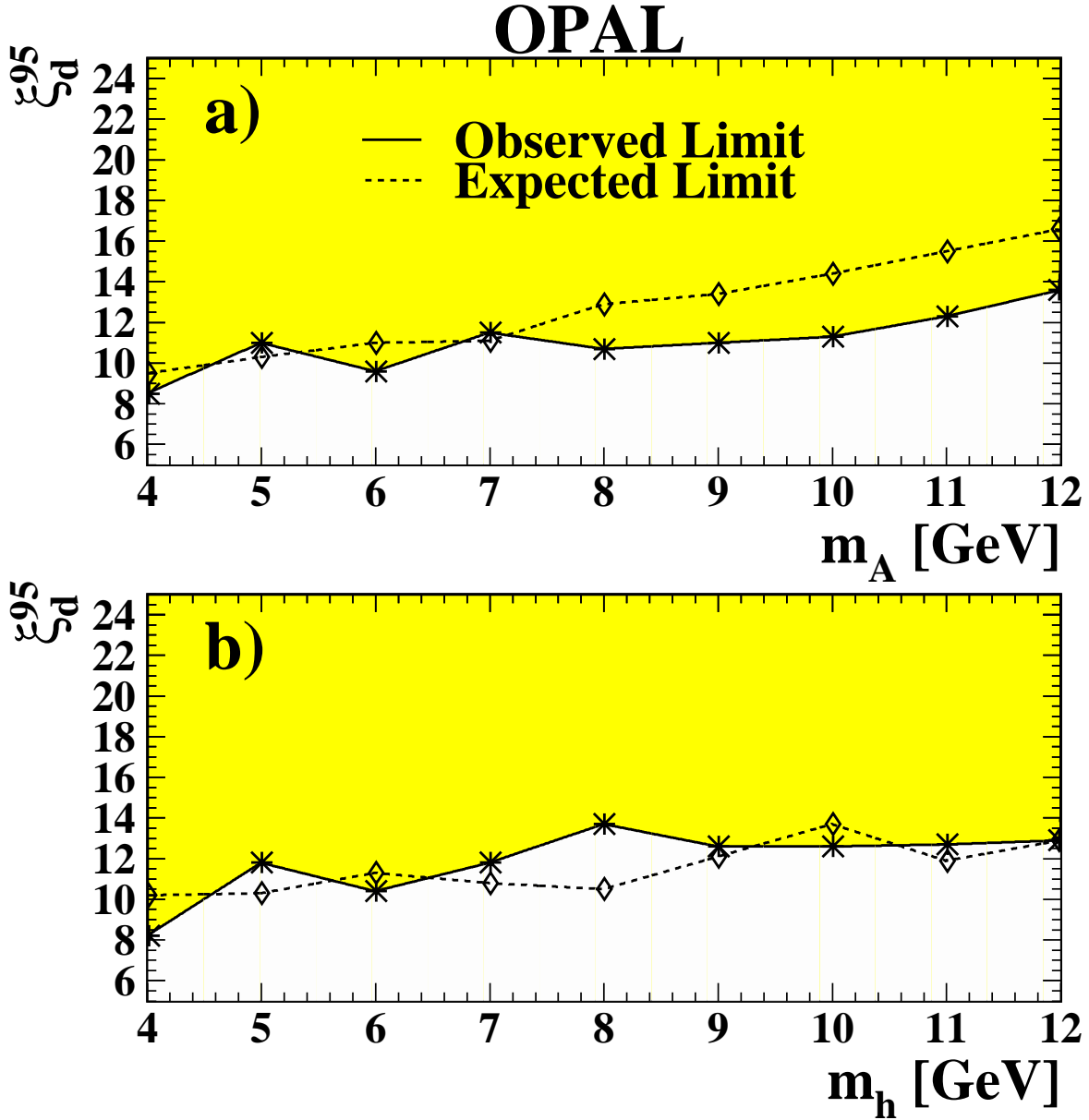


Figure 8: Excluded values of ξ_d at 95% C.L. (dark grey region) in the 2HDM type II model for the Yukawa production of a CP-odd A (upper plot) and for the CP-even h (lower plot) assuming the branching fraction of the Higgs boson into $\tau^+\tau^-$ to be 100%. The expected (diamonds) and observed (stars) limits have been calculated at specific mass points (4–12 GeV in one GeV steps) and linearly interpolated in between.

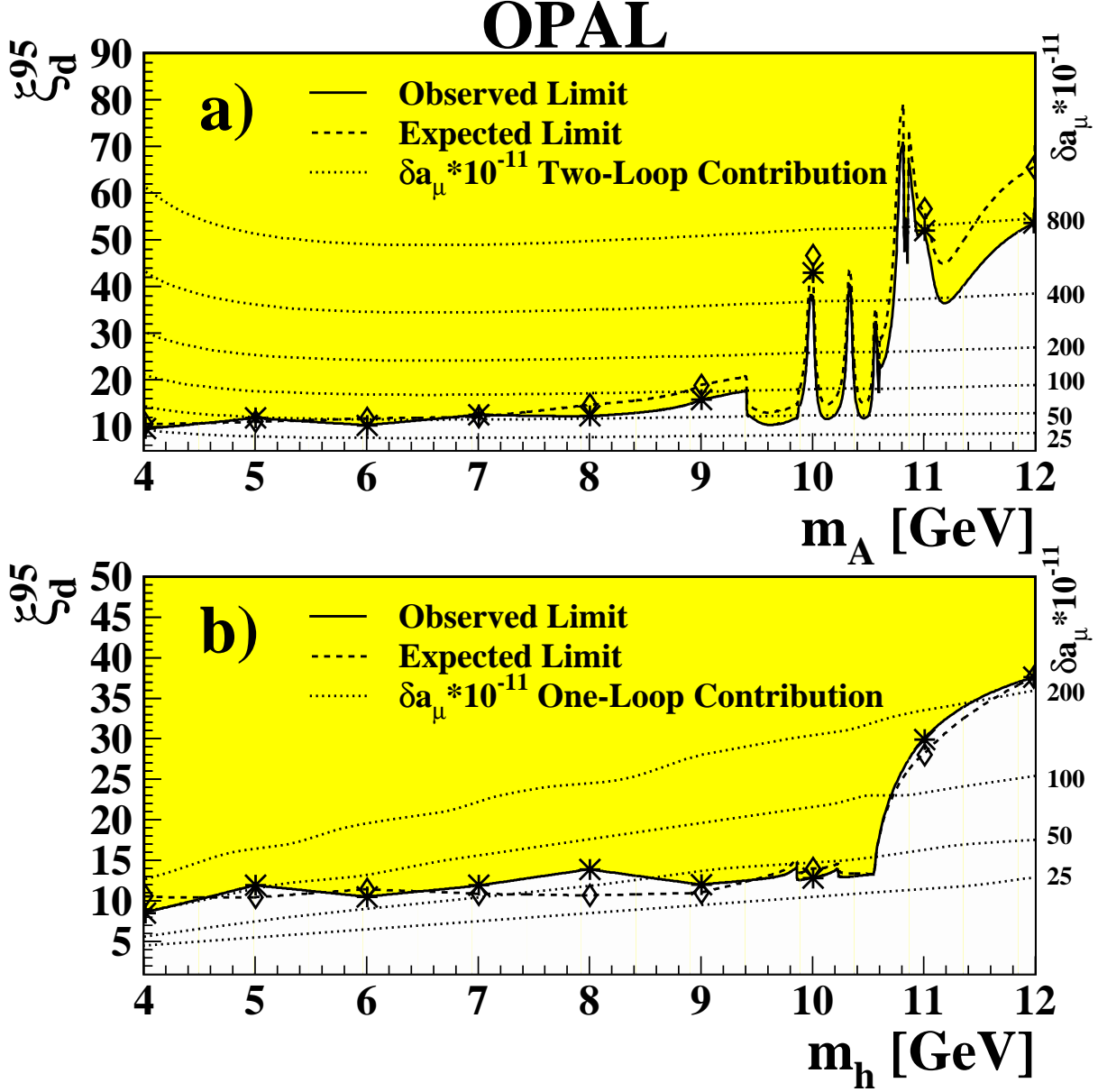


Figure 9: Excluded values of ξ_d at 95% C.L. in the 2HDM type II model with Standard Model particle content for the Yukawa production of a CP-odd A (upper plot) and for the CP-even h (lower plot) with the mixing to $b\bar{b}$ bound states taken into account. The structure results entirely from the theoretically suggested branching ratios [33]. The expected (diamonds) and observed (stars) limits have been calculated at specific mass points (4–12 GeV in one GeV steps) and linearly interpolated in between. The dotted lines are the contours of the predicted Higgs contribution (one-loop [38, 41] for the CP-even and two-loop [39, 40] for the CP-odd Higgs) to the muon anomalous magnetic moment, $\delta a_\mu(\text{Higgs})$ (in units of 10^{-11}).